Nonlinear optical beam propagation for optical limiting

Dmitriy I. Kovsh, Sidney Yang, David J. Hagan, and Eric W. Van Stryland

We implement numerical modeling of high-energy laser-pulse propagation through bulk nonlinear optical materials using focused beams. An executable program with a graphical user interface is made available to researchers for modeling the propagation of beams through materials much thicker than the diffraction length (up to 10^3 times longer). Ultrafast nonlinearities of the bound-electronic Kerr effect and two-photon absorption as well as time-dependent excited-state and thermal nonlinearities are taken into account. The hydrodynamic equations describing the rarefaction of the medium that is due to heating are solved to determine thermal index changes for nanosecond laser pulses. We also show how this effect can be simplified in some cases by an approximation that assumes instantaneous expansion (so-called thermal lensing approximation). Comparisons of numerical results with several *Z*-scan, optical limiting and beam distortion experiments are presented. Possible application to optimization of a passive optical limiter design is discussed.

OCIS codes: 190.5530, 190.5940, 190.4870, 190.3270, 190.4180.

1. Introduction

With the rapid advances in low-cost computer technology, numerical modeling of pulsed laser beam propagation through nonlinear optical (NLO) materials is becoming a powerful tool for investigating the interaction of light with matter. In addition, this modeling is now progressing to the stage where NLO device design can realistically be performed numerically. A variety of algorithms have already been developed and implemented in different areas of optical science, including propagation in waveguide structures[1] and fibers,[2,3] the atmosphere,[4] NLO materials,[5] and in laser cavity design.[6] In this paper we focus on the numerical simulation of high-energy laser beam propagation in bulk NLO media primarily aimed at passive optical limiting applications.[7] There are several difficulties associated with this task. First, the propagation distance through the samples under consideration is up to 2–3 orders of magnitude larger than a Rayleigh length (depth of focus) of the input beam; thus the beam size experiences significant changes along the propagation distance. However, the numerical sampling of the electrical field must be kept fine to accommodate for the large variation of the beam irradiance (that is due to the nonlinear absorption) or the induced phase (that is due to the nonlinear refraction). Second, the additional equations describing the dynamics of the nonlinear response (system of rate equations, acoustic-wave equation, etc.) must be solved in parallel to the electromagnetic wave equation. This leads to rather computationally intense coding and requires large amounts of memory storage (because the spatial profile of the optical susceptibility has to be stored for each time within an optical pulse). Therefore, until recently, the simulations of high-energy laser beam propagation through bulk NLO materials were performed only on high-end workstations or supercomputers.

The main objective of our research is to develop a set of computer codes that will allow us to determine the influence of different nonlinear mechanisms and their coupling on the self-action of the propagating beam. For this purpose, and to allow user-friendly access to such modeling capabilities, we developed a program based on Windows 95/NT, named NLO_BPM.[8] This program models the propagation of the laser pulse through a typical system (Fig. 1), where the sample can be comprised of one or a few NLO elements. One of the ultimate uses of this code is to design passive optical limiting devices.[7] The current capabilities allow the user to propagate picosecond pulses to microsecond pulses through bulk media having a thickness of up to 10^3 times the diffraction length. It also has the capability to model trains of picosecond pulses, typical of those emitted by *Q*-switched, mode-locked lasers, and multiple non-

The authors are with the School of Optics, Center for Research and Education in Optics and Lasers, University of Central Florida, 4000 Central Florida Boulevard, Orlando, Florida 32816-2700.

Received 18 February 1999; revised manuscript received 26 May 1999.

0003-6935/99/245168-13$15.00/0

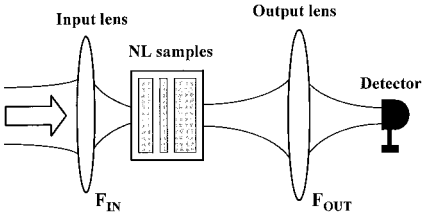

Fig. 1. Typical layout of the system under investigation.

linear elements as in a tandem optical limiting device.

Taking advantage of the cylindrical symmetry of common optical systems (e.g., TEM_{00} laser mode or flat-top beam) allows us to save computer time and memory by reducing the four-dimensional (three dimensions in space and one dimension in time) problem to three dimensions (two dimensions in space and one dimension in time). This also allows us to use PC's to perform calculations on considerably more complicated materials and limiting geometries. (Reference 9 describes another propagation code developed for high-end computer systems that solves noncylindrical symmetry problems but is restricted in the nonlinearities it models, e.g., saturable absorption and thermal diffusion.) Assuming the pulse width is long enough and the propagation distance is short enough that we can ignore the dispersion of the material, the modeling of the beam self-action can be split into two separate tasks. (This is an excellent approximation for the nanosecond and picosecond pulse systems under study.) The first of these tasks is the computing (and storing) of the spatial distribution of the nonlinear susceptibility within the sample for each particular moment in time. The second task is the propagation of each time slice Δt (the nonlinear susceptibility is assumed unchanging within Δt) through the material.

In Section 2 we describe the numerical methods that we used to solve the paraxial wave equation in the nonlinear media. In Section 3 the different nonlinear mechanisms modeled in our code are described. These mechanisms include the Kerr-like nonlinear index (assumed instantaneous), two-photon absorption (2PA), excited-state absorption (ESA), and excited-state refraction in multilevel systems as well as the refractive-index change that is due to thermal expansion. We give examples of calculations of beam propagation through materials with these types of optical nonlinearities. We then show results of modeling and compare the numerical outputs to Z-scan,[10] optical limiting and beam distortion measurements.

2. Beam Propagation Algorithm

The propagation of light through optical media can be described by the solution to the vector wave equation (e.g., Ref. 11):

$$\nabla \times \nabla \times \mathbf{E}(r, t) + \frac{1}{c^2}\frac{\partial^2 \mathbf{E}(r, t)}{\partial t^2} = -\mu_0 \frac{\partial^2 \mathbf{P}(r, t)}{\partial t^2}, \quad (2.1)$$

where $\mathbf{E}(r, t)$ and $\mathbf{P}(r, t)$ are the electric field and medium polarization, respectively. If the laser-pulse duration is much longer than an optical cycle, and the nonlinearity changes slowly compared to an optical oscillation rate, Eq. (2.1) can be simplified assuming that the pulse envelope in time is slowly varying compared to an optical cycle. This results in

$$-\nabla^2 E(r, t) + \frac{(1 + \chi_L)}{c^2}\left[2j\omega \frac{\partial E(r, t)}{\partial t} - \omega^2 E(r, t)\right] = -\mu_0 \omega^2 P_{\mathrm{NL}}(r, t), \quad (2.2)$$

where we used $\mathbf{E}(r, t) = \hat{\imath} E(r, t)\exp(j\omega t)$, $\mathbf{P}(r, t) = \hat{\imath} P(r, t)\exp(j\omega t)$, and $P = \varepsilon_0 \chi_L E + P_{\mathrm{NL}}$, with the assumption that the vector field amplitude and polarization can be treated as scalar quantities ($\hat{\imath}$ is a unit vector). The slowly varying envelope (in time) approximation assumes that

$$\left|\frac{\partial^2 E}{\partial t^2}\right| \ll 2\omega \left|\frac{\partial E}{\partial t}\right|.$$

We also ignore dispersion[2] because our analysis is for laser pulses longer than a few picoseconds, and thus the propagation length L is much longer than the dispersion length $L_D = \tau_p{}^2/|\beta_2|$ (where β_2 is the group-velocity dispersion). Note that Eq. (2.2) does not generally require the pulse envelope to be slowly varying along the direction of propagation z, allowing tight focusing to be included. However, for a slow (i.e., large f-number) optical system, Eq. (2.2) can be greatly simplified by use of the paraxial approximation and, after further transformation of the coordinates to a frame moving at the light phase velocity, Eq. (2.2) can be rewritten in the following form:

$$2jk \frac{\partial \Psi(r, z, t)}{\partial z} = \nabla_\perp{}^2 \Psi(r, z, t) + [k_0{}^2 \chi_{\mathrm{NL}}(r, z, t) - jk\alpha_L]\Psi(r, z, t), \quad (2.3)$$

where $E(r, t) = \Psi(r, z, t)\exp(-jkz)$, $P_{\mathrm{NL}}(r, t) = \varepsilon_0 \chi_{\mathrm{NL}}(r, z, t, E)E(r, z, t)$, and the paraxial approximation is valid when

$$\left|\frac{\partial^2 \Psi}{\partial z^2}\right| \ll 2k \left|\frac{\partial \Psi}{\partial z}\right|.$$

Here $\nabla_\perp{}^2$ and r denote the transverse Laplace operator and radial spatial coordinate, whereas $k = n_0 k_0 = n_0 \omega/c$ is the wave vector in the medium with linear index of refraction $n_0 = (1 + \mathrm{Re}\{\chi_L\})^{1/2}$ and linear absorption $\alpha_L = -(k_0/n_0)\mathrm{Im}\{\chi_L\}$. The paraxial approximation narrows the task to modeling only relatively weakly focused beams [e.g., use of Eq. (2.3) for modeling the propagation of a plane wave whose wave vector forms an angle of 25 deg with respect to the z axis results in a phase error of $\cong 5\%$[12]]. For Gaussian beams, the beam size at the waist should be much larger than a wavelength for the paraxial wave approximation to be valid.[13] (Numerical algorithms implementing nonparaxial beam propagation have

also been developed, but are still at the stage of testing and are beyond the scope of this paper.)

$\chi_{NL}(r, z, t)$ is the nonlinear susceptibility of the material, which may consist of instantaneous and cumulative parts:

$$\chi_{NL}(r, z, t) = \chi_{NL}^{ins}(r, z) + \chi_{NL}^{cum}(r, z, t). \quad (2.4)$$

Equation (2.3) is written in a moving coordinate system and therefore has no explicit time dependence, although the field amplitude as well as the nonlinear susceptibility are, in general, functions of time. Hence the modeling of the laser-pulse propagation in the nonlinear medium can be split into two separate numerical tasks. The first task is dividing the pulse into a number of time slices $\Psi(r, t_n) = \Psi^n(r)$ and propagating each slice as if it were a continuous-wave (cw) beam. The second task is computing and storing the cumulative part of the nonlinear susceptibility that is being induced by each slice $\chi_{NL}(r, z, t_n) = \chi_{NL}^{n}(r, z)$. Therefore the solution to the original time-dependent wave equation [Eq. (2.3)] is converted to a cw propagation problem.

There are a variety of methods dealing with the cw paraxial wave equation. Here we use the beam propagation method, which requires recomputing the transverse field distribution along the direction of propagation z using the formal solution to Eq. (2.3):

$$\Psi(r, z + \Delta z) = \exp[-j\hat{S}(r, z)\Delta z]\Psi(r, z), \quad (2.5)$$

with the propagation operator

$$\hat{S}(r, z) = \frac{1}{2k}\left[\frac{\partial^2}{\partial r^2} + \frac{1}{r}\frac{\partial}{\partial r} + k_0^2\chi_{NL}(r, z) - jk\alpha_L\right]. \quad (2.6)$$

For simplicity, we henceforth combine the linear absorption and nonlinear susceptibility into a new parameter, $\chi_{NL}'(r, z)$, where

$$\chi_{NL}'(r, z) = \chi_{NL}(r, z) - j\frac{n_0}{k_0}\alpha_L. \quad (2.7)$$

We use two algorithms to numerically solve Eqs. (2.4)–(2.7). First is the spectral method (SM) suggested by Feit and Fleck[3] that uses a formal expansion of the propagation operator (2.5) into a Taylor series and one-dimensional fast Fourier transform to evaluate the radial derivatives in Eq. (2.6). The second algorithm is the Crank–Nicholson finite difference method (FDM) reformulated for cylindrical coordinates which is commonly applied to solve parabolic differential equations (e.g., the time-dependent Schrodinger equation). The FDM is accurate to second order in Δz and Δr.[14,15] We keep the same order of accuracy in the SM by neglecting higher expansion terms of Eq. (2.5). The SM, although not unitary, yields accurate results if the step size Δz is chosen to be small enough (in our calculations this must be of the order of a few optical wavelengths).[3] The second algorithm is unitary and unconditionally stable in the linear case, therefore it is less restrictive on the choice of Δz. We can increase the accuracy of the SM beyond $O(\Delta z^3)$ by including higher-order terms in the expansion of the propagation operator in Eq. (2.5).[3,16] This will, however, increase the computation time. Thus we primarily use the Crank–Nicholson algorithm for its robustness and efficiency. We also find that the requirement on radial sampling size is less strict for the SM than for the FDM, thus allowing fewer sampling points to be used. The radial sampling size in the SM is defined so that aliasing does not occur. (There should be at least two sampling points per cycle to avoid aliasing.[14]) The choice of Δr in the FDM is dictated by the condition that the phase difference between adjacent points be less than a fraction of π radians (e.g., $\pi/10$). For the parabolic phase front (typical for Gaussian beams) this results in $\Delta r < \lambda z/(20w)$, where z is the distance from the focus and w is the maximum radial beam size. Overall, the SM is to be used for tasks that require higher (than third-order) accuracy and when the CPU time is not a critical issue; however, we suggest using the FDM in most cases for its speed.

The developed algorithms allow us to save computer memory by use of only two-dimensional arrays of data to store the complex electric field amplitude $\Psi(r, t)$ and by use of cylindrical symmetry of the system. At the same time, the cumulative part of the nonlinear susceptibility has to be saved as a function of spatial coordinates r and z and be updated after every time slice propagates through the sample. However, these two-dimensional arrays representing $\chi_{NL}^{cum}(r, z)$ for a particular moment in time can have a sampling step size Δz_{NL} along z that is considerably larger than the propagation step size Δz if the cumulative nonlinearity is a more slowly changing function of z than the field distribution. It is convenient to have Δz_{NL} be a multiple number of Δz.

The methods chosen to model the cw beam propagation are efficient, allowing us to model the propagation of the beam through distances of tens or even hundreds of diffraction lengths, while the beam changes its size by several orders of magnitude. To test both methods we modeled the free-space propagation of the cw Gaussian beam (beam size at the waist, $w_0 = 8$ μm; wavelength, $\lambda = 532$ nm) through 40 Rayleigh ranges (z_0) starting at the position $20z_0$ before the waist. The accuracy of the modeling was checked by a comparison of the beam size $w(z)$ (calculated as the second moment of irradiance] and the power $P(z)$ with the analytical values. We kept the radial sampling step constant (although the number of points varied depending on the beam size). The largest error occurred at the waist where the number of sampling points is the smallest (128 points). In this test we found that generally the FDM is approximately 8–10 times faster than the SM for the same accuracy in estimating $w(z)$ and $P(z)$ (the error was kept below 0.2%). The CPU time for a Pentium II 300-MHz computer was approximately 3.5 and 30 s for the FDM and SM, respectively. (Note that absolute values of the CPU times include the time for outputting to data files, etc., so that the ratio between the CPU times is the more meaningful number.)

The sampling step along z in the FDM was ten times greater than in the SM($\Delta z \sim 6\lambda$ for the SM); however, the radial sampling step was four times smaller for SM($\Delta r \sim 3\lambda$ for the SM). Options for both the SM and the FDM are included in the NLO_BPM code.[8]

3. Nonlinear Mechanisms

The nonlinear susceptibility as given in Eq. (2.4) is related to the nonlinear refractive-index change Δn and the absorption of the material as

$$\mathrm{Re}\{\chi_{\mathrm{NL}}'(r, z)\} = 2n_0\Delta n(r, z), \tag{3.1a}$$

$$\mathrm{Im}\{\chi_{\mathrm{NL}}'(r, z)\} = -\frac{n_0}{k_0}\alpha(r, z) = -\frac{n_0}{k_0}[\alpha_L + \alpha_{\mathrm{NL}}(r, z)]. \tag{3.1b}$$

Here α_L is the linear absorption coefficient and $\alpha_{\mathrm{NL}}(r, z)$ is the nonlinear absorption coefficient of the material.

A. Instantaneous Nonlinearities

If the nonlinear response of the material has a characteristic time much shorter than the pulse width (for our purposes shorter than a few picoseconds), then we can consider it to be instantaneous and it can be described by the first term of the nonlinear susceptibility in Eq. (2.4). Typical examples of such nonlinearities are the bound-electronic nonlinear Kerr effect [nonlinear refractive index n_2, as defined in Eq. (3.2) below] and 2PA (coefficient β_2). The relations for these quantities are

$$\Delta n(r, z) = n_2 I(r, z), \tag{3.2}$$

$$\alpha_{\mathrm{NL}}(r, z) = \beta_2 I(r, z). \tag{3.3}$$

To demonstrate the usefulness of the beam propagation codes, we show the results of modeling a thick-sample Z-scan experiment for materials exhibiting only an instantaneous nonlinear response. Figure 2 shows an open-aperture Z-scan of a two-photon absorber ($\beta_2 = 6$ cm/GW) and a closed-aperture Z-scan of CS_2 ($n_2 = 3.1 \times 10^{-5}$ cm^2/GW) both obtained by use of a Gaussian beam focused to an 8-μm spot size (HW1/e^{2}M of irradiance) and a pulse width of 20 ps (HW1/eM of irradiance). The thickness of the sample in both cases was 1 cm, which is 16 times longer than the Rayleigh range of the Gaussian beam inside the material ($26.5z_0$ in air). The CPU time to calculate each point in the Z-scans was approximately 13 s for the Pentium II 300-MHz computer (five slices in time were used).

B. Excited-State Nonlinearities

ESA is a well-known two-step process. An absorption process creates population in an excited state (for semiconductors these are free carriers), which subsequently absorbs light linearly to some higher state (free-carrier absorption in semiconductors). The initial absorption process can be linear or nonlinear; however, we first discuss the case of linear excitation of the excited state with ground-state absorption

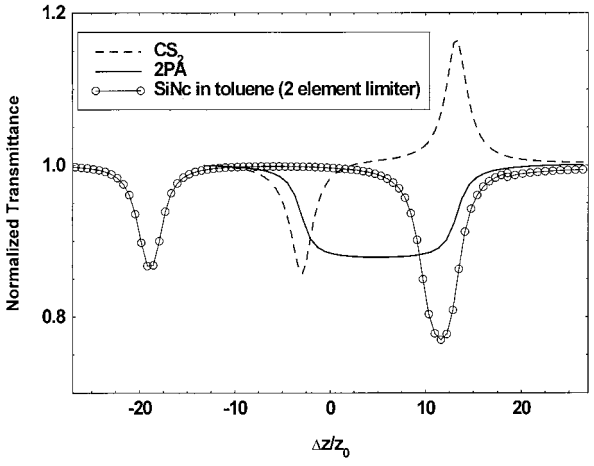

Fig. 2. Thick-sample Z-scan. Closed-aperture Z-scan of CS_2 ($n_2 = 3.1 \times 10^{-5}$ cm^2/GW), open-aperture Z-scan of 2PA ($\beta_2 = 6$ cm/GW), and open-aperture Z-scan of a two-element optical limiter. Thickness of the sample is 1 cm ($26.5z_0$ in air). The two-element tandem limiter is based on a toluene solution of SiNc (thickness of the cells is $L_1 = 2$ mm, $L_2 = 1$ mm; separation $S = 7$ mm).

cross section σ_G. This results in an overall third-order nonlinear absorption process.[17–19] Depending on whether the ESA cross section σ_e is smaller or larger than σ_G, we can distinguish saturable absorption ($\sigma_G > \sigma_e$) from reverse saturable absorption (RSA) ($\sigma_G < \sigma_e$). RSA was shown[18,20] to be a promising nonlinearity for passive optical limiters (devices that are transparent for low-energy inputs but exhibit low transmittance for high-energy inputs[7]) because the material becomes highly absorptive as the input fluence (energy per unit area or time-integrated irradiance) of the beam increases. Because this nonlinear effect accumulates in time, this nonlinearity is often more effective for longer pulses than instantaneous nonlinearities (i.e., fast response with no memory). Several organic materials exhibit RSA properties in the visible region, including several porphyrin dyes, phthalocyanines, naphthalocyanines and their derivatives, as well as polymethine dyes.[19,21] The energy-level structure of these materials can be well approximated by a five-level model (see Fig. 3) where the G–S_1 transition represents the linear absorption and S_1–S_2, or T_0–T_1, represent the ESA. Time constants and cross-sectional values were experimentally investigated for Zn:tetra(p-methoxyphenyl)benzporphyrin (TBP), silicon naphthalocyanine (SiNc), lead phthalocyanine (PbPc), and several other materials.[17,18]

The overall absorption of the system can be derived as a function of the populations of the levels:

$$\alpha = \sigma_G N_G + \sigma_S N_{S_1} + \sigma_T N_{T_1}, \tag{3.4}$$

where σ_S or $\sigma_T > \sigma_G$ for RSA. The dynamics of the five-level system can be described by a set of five rate equations[19] that usually can be simplified for a particular time scale of the laser pulse to reduce the computation time.[16,20] For nanosecond pulses, a

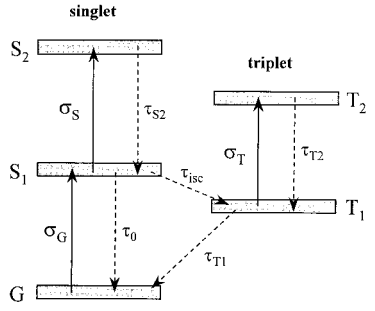

Fig. 3. Five-level system. For SiNc, $\sigma_G = 2.8 \times 10^{-18}$ cm^2, $\sigma_S = 40 \times 10^{-18}$ cm^2, $\sigma_T = 120 \times 10^{-18}$ cm^2, $\tau_0 = 1.6$ ns, $\tau_{\text{isc}} = 6.5$ ns, $\tau_{S_2} = 1.3$ ps, and $\tau_{T_1} = 0.3$ μs.

good approximation is obtained by one assuming the decay time of levels S_2 and T_2 to be much smaller than the pulse width (usually τ_{S_2} and τ_{T_2} are of the order of a few picoseconds or less). This eliminates the need for tracking the populations of levels S_2 and T_2 because their populations remain near zero. Also if the decay time of the first triplet level τ_{T_1} is much longer than the pulse width, it can be taken as infinite. These simplifications result in

$$\frac{\mathrm{d}N_{S_1}}{\mathrm{d}t} = \sigma_G N_G \frac{I}{\hbar\omega} - \frac{N_{S_1}}{\tau_{S_1}},$$

$$\frac{\mathrm{d}N_{T_1}}{\mathrm{d}t} = \frac{N_{S_1}}{\tau_{\text{isc}}},$$

$$N_G + N_{S_1} + N_{T_1} = N_0. \tag{3.5}$$

Here the overall decay rate of S_1 is $1/\tau_{S_1} = 1/\tau_0 + 1/\tau_{\text{isc}}$, where τ_{isc} is the intersystem crossing time that characterizes the dynamics of decay from the singlet manifold to the triplet manifold. In some molecular systems τ_{isc} could represent a *cis–trans* transition (e.g., in polymethine dyes[21]). The triplet yield is given by $\phi = \tau_{S_1}/\tau_{\text{isc}}$ and N_0 is the total density of molecules (atoms or ions). If the laser pulse is in the range of tens of picoseconds, decay to the triplet manifold can often be entirely ignored because $\tau_{\text{isc}} \gg \tau_p$, and thus the five-level system can be reduced to a three-level system. In this case, and assuming no saturation of level S_2, the three-level system has an analytical solution.[16,20] To illustrate the utility of the developed beam propagation method codes, we show the result of modeling a Z-scan experiment[10] with a two-element tandem optical limiter based on a toluene solution of SiNc (in Fig. 2, experimental parameters are taken from Ref. 7). Such experiments help to define the position of the focal plane of the system under investigation.

Because such materials exhibit ESA, they normally show excited-state refraction as well. This is a consequence of the redistribution of population changing the absorption spectrum, which by causality (resulting in Kramers–Kronig relations[22]) changes the refractive index. However, the magnitude (and sign) of this nonlinear refraction has a different frequency dependence from that of the nonlinear absorption. This nonlinear refractive-index change has been observed for several materials and it is proportional to the density of excited states (or free carriers). Mathematically this can be represented by refractive cross sections, defined by[16]

$$\Delta n = \frac{\sigma_{S_{1,r}} N_{S_1} + \sigma_{T_{1,r}} N_{T_1}}{k}, \tag{3.6}$$

where $\sigma_{S_{1,r}}$ and $\sigma_{T_{1,r}}$ are refractive cross sections of the first singlet and triplet levels.

C. Thermal Effects

A laser pulse, while passing through absorbing media, induces temperature and density gradients that change the refractive-index profile. This process is often called the thermal lensing effect because the change in refractive index usually follows the beam shape, thus forming a lens within the medium. This phenomenon has been rigorously studied both experimentally[23–25] and theoretically.[26–34] The heat deposited in the material by absorption of light determines the temperature gradient that may change according to thermal diffusion. Steady-state, diffusion-dominated thermal lensing was investigated in Refs. 26–28. The density changes that result from the temperature gradient (or by electrostriction induced by the gradient of the electric field of the laser beam[11]), are transmitted at the speed of sound as described by the acoustic-wave equation.[29,30] Hence, for various time scales the thermal effect has different manifestations.

If the pulse width is longer than a few microseconds, the heating of the material can be described by the following diffusion equation giving the temperature distribution in space and time[30]:

$$\rho c_p \frac{\partial T}{\partial t} - \kappa \nabla^2 T = \alpha_L I, \tag{3.7}$$

where ρ is the density of the medium, c_p is the specific heat at constant pressure, κ is the thermal conductivity, and $\alpha_L I$ is the portion of the laser power transformed to heat. However, in this paper we are working on time scales short enough (up to a few tens of nanoseconds) that diffusion can be ignored, and thus the temperature change induced by laser radiation can be estimated for any spatial position as

$$\Delta T(t) = \frac{1}{\rho c_p} \int_0^t \alpha_L I(t')\mathrm{d}t'. \tag{3.7a}$$

In general, the refractive-index change is a function of both temperature and density changes inside the material:

$$\Delta n = \left(\frac{\partial n}{\partial \rho}\right)_T \Delta\rho + \left(\frac{\partial n}{\partial T}\right)_\rho \Delta T. \tag{3.8}$$

Here $(\partial n/\partial\rho)_T$ describes the index changes that are due to rarefaction or compression of the medium, which could be a result of heating or of electrostric-

tion. $(\partial n/\partial T)_\rho$ may include a variation of index that is due to other temperature-induced changes in the material, such as, for example, changes in the bandgap energy.[16] These other effects are often dominant in solids, but in liquids, density changes usually dominate. For longer times, ignoring electrostriction, $\Delta\rho = (\partial\rho/\partial T)_p \Delta T$, where the derivative $(\partial\rho/\partial T)_p$ is a constant of the material. Because our interest is driven by optical limiting, we often work with strongly absorbing liquids in which case electrostriction is dominated by thermal effects. This is generally not the case for solid media in which the thermal refractive-index variations are usually an order of magnitude smaller than in liquids and often can be masked by the electrostrictive effect.[35,36] In what follows we concentrate on liquids and ignore the electrostrictive effect. However, it should be noted that modeling of the thermal effect easily allows for modeling of electrostriction and both are included in the NLO_BPM code.

On a nanosecond time scale, refractive-index variations that are due to expansion of the medium generated by local heating (absorptive mode) or by compression that is due to the electromagnetic field of the laser beam (electrostrictive mode) are highly transient. According to the derivation given in Appendix A, the thermal index change induced by propagation of a nanosecond laser pulse through a liquid can be described by the following acoustic-wave equation:

$$\nabla^2(\Delta n) - \frac{1}{C_S{}^2}\frac{\partial^2(\Delta n)}{\partial t^2} = -\frac{\gamma^e \beta}{2n}\nabla^2(\Delta T), \qquad (3.9)$$

where C_S is the velocity of sound, β is the thermal expansion coefficient, and γ^e is the electrostrictive coupling constant. For typical values of the sound velocity in liquids (C_S = 1–2 μm/ns), if we have a few nanosecond-long pulses focused to a spot size, w = 10–20 μm, only later portions of the pulse experience the index changes induced by the front part of the same pulse. In such a case, where the acoustic transit time $\tau_{ac} = w/C_S$ is greater than the pulse width, we must solve Eq. (3.9). However, in cases in which τ_{ac} is somewhat less than the pulse width, we can simplify the numerical modeling of this photoacoustic effect by parameterizing the index change close to the propagation axis by the following expression (essentially assuming an instantaneous expansion):

$$\Delta n \cong \left(\frac{\mathrm{d}n}{\mathrm{d}T}\right)_0 \Delta T, \qquad (3.10)$$

where $(\mathrm{d}n/\mathrm{d}T)_0 = \gamma^e\beta/2n$ is called the thermo-optic constant. With such a approximation we can significantly reduce the computational time required to numerically solve the acoustic-wave equation for each time slice of the pulse. In fact, there are experimental results in the literature where the thermo-optic coefficient was calculated with this approximation for different liquids.[38–40]

To verify the validity of such an approximation, we present in Fig. 4 the results of modeling the propagation of a 10-ns (HW1/eM of irradiance) pulse with a Gaussian spatial profile (beam size at the waist is w_0 = 6 μm, HW1/e^{2}M of irradiance) through a water solution of nigrosine dye (linear transmittance T_L = 90%, thickness L = 200 μm). Nigrosine is chosen because it shows little nonlinear response other than thermal refraction induced by linear absorption for nanosecond inputs. The closed-aperture Z-scan signals computed with and without approximation (3.10) show excellent agreement with each other.

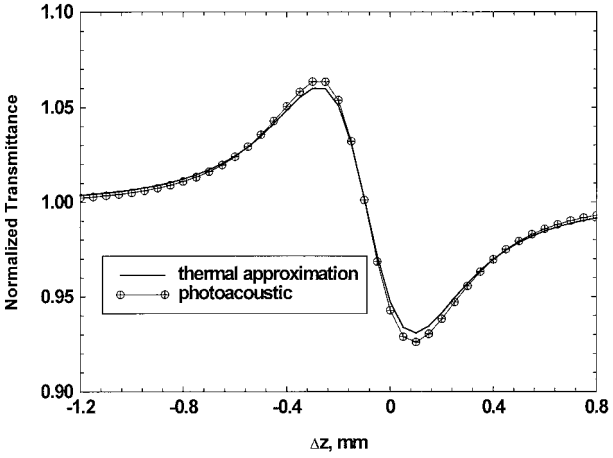

Fig. 4. Closed-aperture Z-scan of nigrosine solution in water. Nonlinear refractive-index change was computed as a solution to the acoustic equation and its approximation. Parameters of the laser beam are pulse width τ_p = 10 ns (HW1/eM), beam size at the waist w_0 = 6 μm (HW1/e^{2}M), and input energy E_{IN} = 2 μJ. Linear transmittance of the sample T_L = 90% and thickness of the sample L = 200 μm (τ_p/τ_{ac} = 2.5).

Nevertheless, one has to be careful using approximation (3.10) and the experimental data for the effective Δn reported in the literature. For example, if Δn was determined by use of the closed-aperture Z-scan technique with input laser pulses on the nanosecond time scale, the approximation may be violated. Relation (3.10) assumes that the thermal lens is being induced instantaneously and ignores the small-index disturbances on the wings of the beam, which are due to the acoustic-wave propagation.[41] If the beam size is too large and the acoustic wave does not have enough time to grow within the pulse, approximation (3.10) will overestimate the induced index change. Such a discrepancy is shown in Fig. 5, where the waist of a Gaussian beam was increased to w_0 = 30 μm. The input energy was also increased by a factor of 25 to keep the same value of fluence at the focal plane and therefore the same value of the thin-sample closed-aperture Z-scan signal. If this approximation were used to analyze the experimental data (for example Z-scan curves), the value of the thermo-optic coefficient $(\mathrm{d}n/\mathrm{d}T)_0$ would be overestimated as can be seen in Fig. 5. Clearly, approximation (3.10) yields a larger nonlinear phase shift and consequently larger value of the peak-to-valley transmittance ΔT_{P-V}.

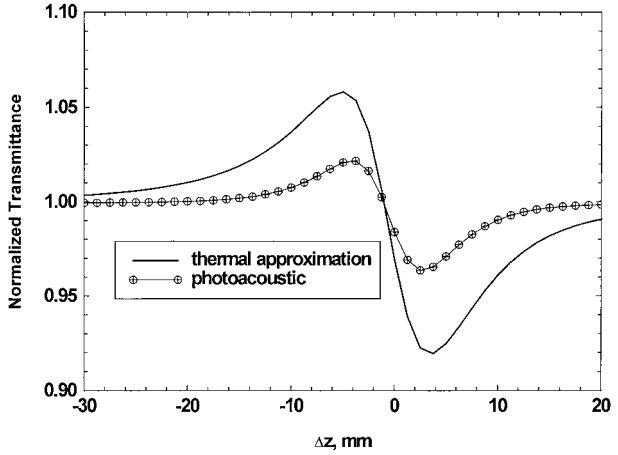

Fig. 5. Closed-aperture Z-scan of nigrosine solution in water. Nonlinear refractive-index change was computed as a solution to the acoustic equation and its approximation. Parameters of the laser beam are $\tau_p = 10$ ns, $w_0 = 30$ μm, and $E_{IN} = 50$ μJ. Linear transmittance of the sample $T_L = 90\%$ and $L = 200$ μm ($\tau_p/\tau_{ac} = 0.5$).

To explore the range of validity of approximation (3.10) even further, we model the closed-aperture Z-scan experiment for different values of the ratio between the pulse width τ_p and the acoustic transit time τ_{ac}, computing the thermal index change Δn as a solution to the photoacoustic-wave equation [Eq. (3.9)]. We then normalize the peak-to-valley change in transmittance ΔT_{P-V}, obtained this way to the ΔT_{P-V} calculated if approximation (3.10) is applied. Repeating this procedure for various values of the pulse width and beam size as well as different input energies, we obtain the same dependence between the ΔT_{P-V} [normalized to the value estimated with relation (3.10)] and τ_p/τ_{ac} shown in Fig. 6. Note that the relation between the thickness of the sample and the beam size satisfied the thin-sample approximation for which the theory of the Z-scan experiment

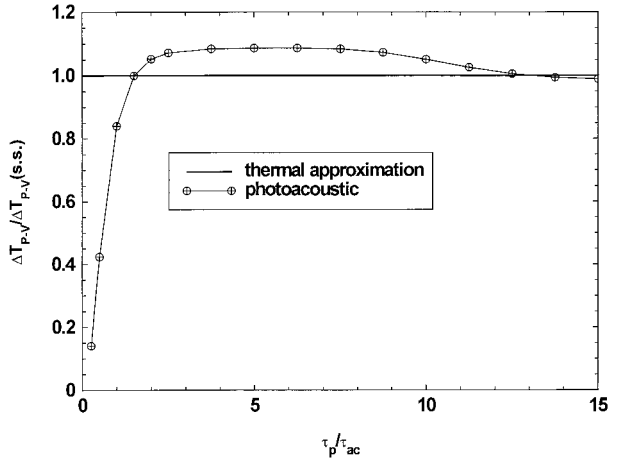

Fig. 6. Sensitivity (ΔT_{P-V}) of the closed-aperture Z scan as a function of ratio between pulse width τ_p and acoustic transit time $\tau_{ac} = w_0/C_S$. ΔT_{P-V} is normalized to the value obtained with the thermal lensing approximation.

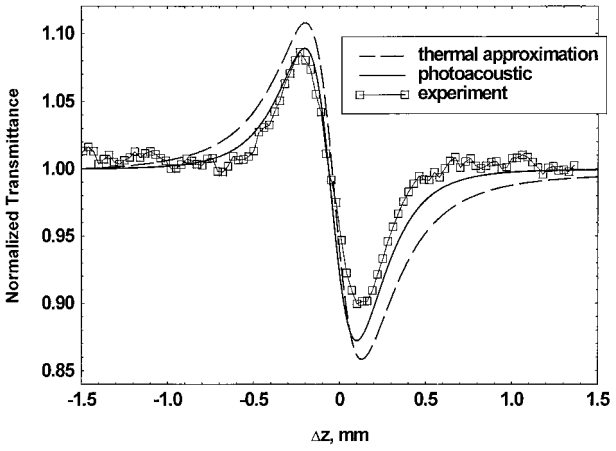

Fig. 7. Closed-aperture Z-scan of nigrosine in water [$\tau_p = 7$ ns (FWHM), $w_0 = 6$ μm, $T_L = 40\%$, $L = 50$ μm, $E_{IN} = 0.55$ μJ]. Comparison between modeling and experimental data.

was derived.[42] Hence we conclude that the ratio τ_p/τ_{ac} can be used to describe the transient photoacoustic effect, and approximation (3.10) is only valid when

$$\frac{\tau_p}{\tau_{ac}} \geq 1.5. \tag{3.11}$$

Note that the values of the ratio τ_p/τ_{ac} for the Z-scans shown in Figs. 4 and 5 are 2.5 and 0.5, respectively, which explains why approximation (3.10) works for the first case ($\tau_p/\tau_{ac} = 2.5$) and fails to work for the second ($\tau_p/\tau_{ac} = 0.5$). The detailed studies of the thermal transient effects are described in Ref. 41, where we also explain why the solution to the acoustic equation overshoots its steady-state value.

To justify our conclusions we modeled the closed-aperture Z-scan experiment performed with the aqueous solution of nigrosine dye taking the value of the thermo-optic coefficient of water to be $-0.9 \times 10^{-4}\,K^{-1}$.[37] The parameters of the laser pulse ($w_0 = 6$ μm and $\tau_p = 4.2$ ns) give the value 0.94 for the ratio in inequality (3.11), and therefore, according to Fig. 6, approximation (3.10) is expected to slightly overestimate the value of ΔT_{P-V} (by approximately 15%) as can be seen in Fig. 7. However, a good agreement of the modeling with the experimental data is demonstrated if the photoacoustic equation [relation (3.10)] is used to estimate the refractive-index change.

As mentioned above, heating of the material is caused by absorption of the laser beam energy; however, the mechanisms of such absorption can vary. If we consider the source of the thermal nonlinearity to be RSA, we can evaluate the significance of this effect by running the propagation code including RSA only and including both RSA and the thermal effects together. The toluene solution of SiNc was chosen to be the material for this test because all the parameters needed for the numerical modeling are relatively well known.[17,37] For low input energy, thermal refraction has a small effect on the propagation of the 4.6-ns (FWHM) pulse focused to $w_0 = 8$ μm inside the 1-mm-thick sample. (The sample with linear trans-

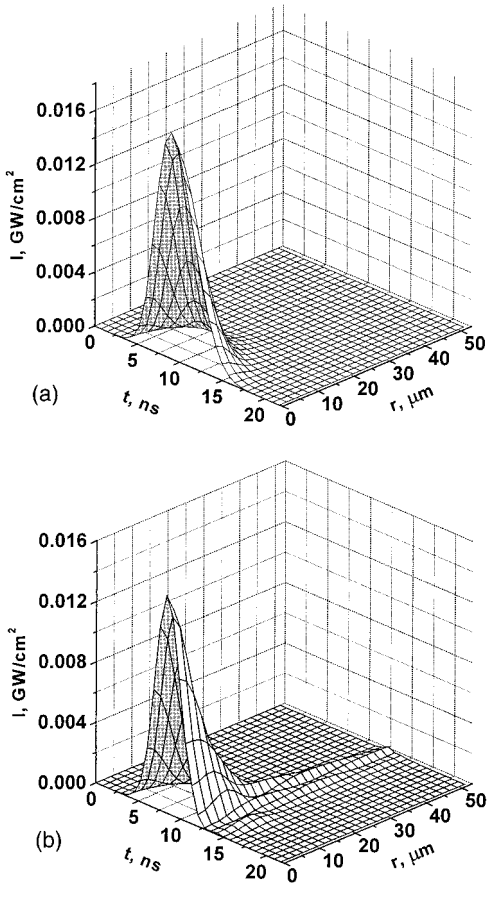

Fig. 8. Modeling of spatial irradiance distribution in the center of the pulse passing through the cell filled with the toluene solution of SiNc [τ_p = 4.6 ns (FWHM), w_0 = 8 μm, T_L = 60%, L = 1 mm, E_{IN} = 2 μJ]: (a) with RSA only and (b) with RSA and thermal refraction.

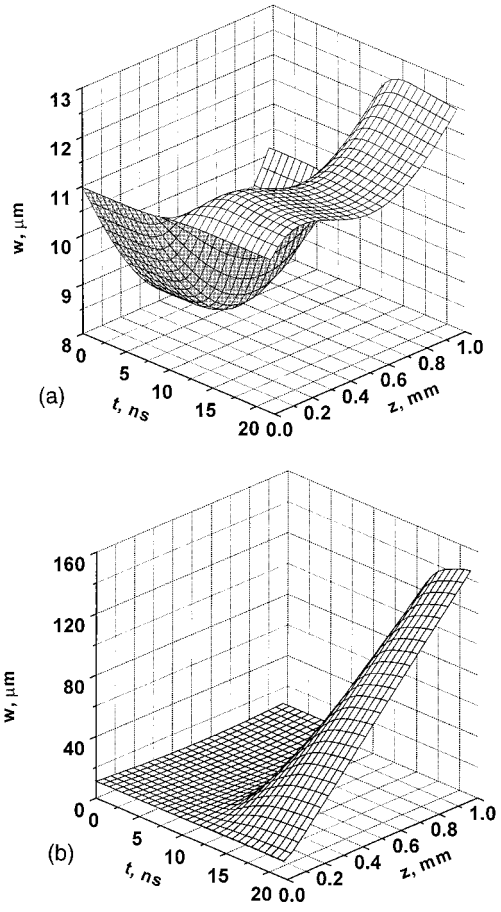

Fig. 9. Beam size (computed as a second moment of irradiance) inside the sample as a function of z and time during the pulse. Parameters of the system are the same as for Fig. 8: (a) with RSA only and (b) with RSA and thermal refraction.

mittance T_L = 60% is placed so that the linear optics beam waist is located at the center of the sample.) Note that the thickness of the sample is approximately three times greater than the Rayleigh range, hence diffraction of the beam has to be considered, requiring the beam-propagation-based numerical approach to tackle the problem. We found that coupling between the refractive-index change and the RSA becomes evident once the input fluence reaches a value of approximately one order of magnitude smaller than the damage threshold of the glass cuvette container (approximately 10 J/cm^2, which corresponds to an input energy of 20 μJ). We chose a value of the input energy, E_{IN} = 2 μJ, to be ten times less than the damage value (it caused a maximum calculated temperature change inside the sample of approximately 70 K). Figure 8 shows the irradiance distribution on the back surface of the sample as a function of time and radial coordinate for the cases when only RSA is included in the modeling [Fig. 8(a)] and when both RSA and thermal effects are taken into account [Fig. 8(b)]. Figure 9 shows the beam size (numerically evaluated as the second moment of irradiance) as a function of time and z coordinate. Clearly, the later parts of the pulse are severely defocused by the thermal effects. Note that the thermal defocusing of the beam for the later times of the pulse aggravates linear defocusing (diffraction) because half of the sample is located after the beam waist. The calculations discussed above are useful when we study the limiting performance of the liquid solutions of RSA materials for nanosecond pulses.

4. Limiting Experiments

Limiting devices based on liquid solutions of organic dyes exhibiting RSA (discussed above) were shown to have high dynamic ranges and reusability.[43] The limiting performance of such absorbers is strictly fluence dependent if the input laser pulse is in the picosecond range. This is due to the ESA introduced by the first singlet level (S_1 in Fig. 3). However, for nanosecond pulses it was reported that the limiting performance of these materials used in tandem limiting geometries is lower than predicted by a five-level model.[7,43] We expect that the primary mechanism responsible for this degradation in performance is the transient thermal refraction caused by local heating[44,45] of the liquid solvent. Another effect that can significantly change the limiting characteristics of such devices for high inputs is nonlinear scatter-

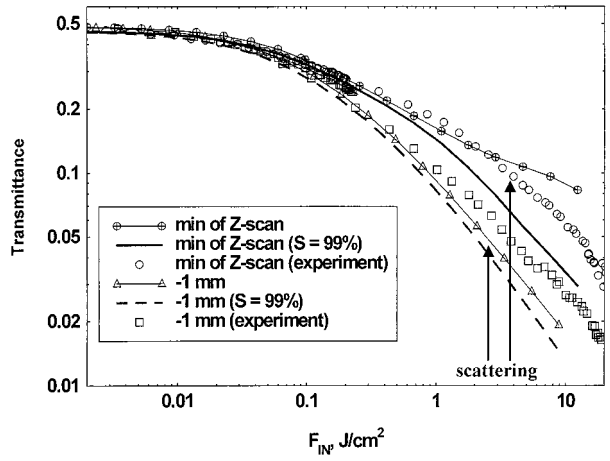

Fig. 10. Limiting curves showing the performance of the 1-mm SiNc–toluene limiter for two positions of the limiting element with respect to the focus as a function of input fluence [$w_0 = 6$ μm, $\tau_p =$ 7 ns (FWHM), $T_L = 48\%$]. Solid curves show the results of modeling if the aperture ($S = 99\%$) is placed in front of the detector. Arrows show the values of input fluence at which the nonlinear scattering becomes noticeable as observed by a detector positioned off to the side of the sample.

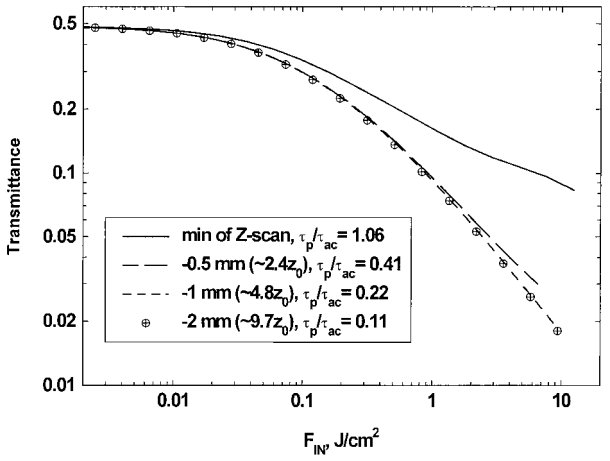

Fig. 11. Limiting performance of the SiNc–toluene limiter for various positions of the sample. Parameters are the same as for Fig. 10.

ing.[46,47] Both effects were experimentally studied and even some phenomenological analysis including the simplified thermal effect was offered. Nevertheless, to analyze the experimental data one needs to combine all relevant self-action mechanisms (including transient effects), and in this case numerical modeling is required. Moreover, if the thickness of the limiter exceeds the depth of focus (Rayleigh range) of the beam (or if the nonlinear phase distortion becomes large), diffraction within the sample must be included. This often results in coupling of different nonlinear mechanisms with each other and with the diffraction phenomenon. This is especially evident when the input fluence reaches values comparable to the damage threshold of the device. To the best of our knowledge, none of the numerical codes discussed in the literature[9] is capable of modeling this scope of tasks.

Figures 10 and 11 present the results of modeling the performance of an optical limiter based on a toluene solution of SiNc. The transient photoacoustic refraction was included along with RSA in the calculations. The position of the 1-mm-thick ($\sim 3.3 z_0$) sample was varied to study the importance of the thermal effect and its coupling with RSA. We also experimentally detected the values of the input fluence when nonlinear scattering (which has not yet been incorporated in our models) becomes observable (Fig. 10). We experimentally detect scattering by placing a detector off to the side of the sample. The pulse width is 7 ns (FWHM) and the values of the ratio τ_p/τ_{ac} corresponding to the positions of the sample are also shown in Fig. 11 (beam size at the waist is 6 μm). Although no fitting parameters are used in the modeling, the comparison with the experimental data shown in Fig. 10 gives excellent agreement. Here we also assumed that all the absorption goes to heat, ignoring radiative decay from excited singlet and triplet levels. Nonlinear scattering reduces the amount of the absorptive energy transferred to heat and thus, for the purpose of modeling, can be treated as an additional absorption mechanism that does not participate in the thermal equations. Hence the thermal lens predicted by modeling slightly overestimates the experimental one (Fig. 10). Also it is important to emphasize that thermal refraction is critical only if the sample is placed near focus, where the beam size is the smallest. Experimentally we determine this position by running the open-aperture Z-scan experiment and detecting the shift Δz corresponding to the minimum of the Z-scan curve. If the thermal self-action is negligible, the limiting performance, at a fixed fluence, should be the same for all positions of the sample (Fig. 11). This conclusion is especially useful for the design and optimization of limiting devices based on liquid solutions of RSA materials (e.g., tandem limiters). We also observed that the combined effects of thermal refraction and nonlinear scattering noticeably expand the beam passing through the cuvette filled with a toluene solution of SiNc for high values of input fluence. Therefore the aperture of the collecting lens placed behind the sample may clip the beam. To model such clipping we calculated the limiting curves produced with an $S = 99\%$ linear transmittance clipping aperture (also shown in Fig. 10). The value of S (as defined in the Z-scan literature[10,42]) is rather arbitrary and used only to show that the limiting performance will benefit if such an aperture is used. This is due to the fact that thermal defocusing changes the spatial profile of the beam on the detector (or on the collecting optics) to have a large pedestal caused by severe spatial expansion of the later portions of the pulse.

5. Flat-Top Beam Analysis

We also performed experiments and analysis of so-called flat-top beams. We experimentally produce

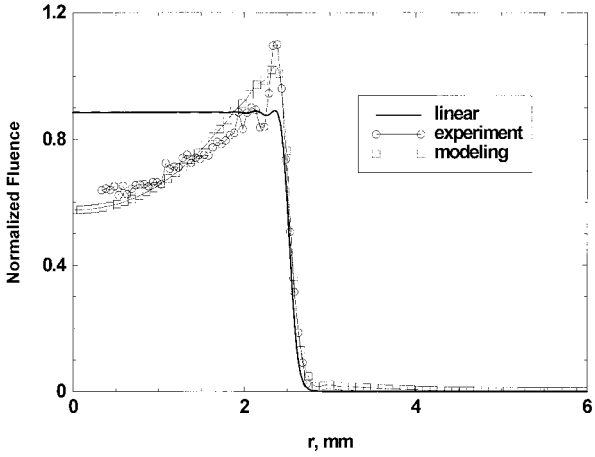

Fig. 12. Normalized radial fluence distribution at the image plane of the system with the flat-top input beam spatial profile [input radius $w_{IN} = 3$ mm, $\tau_p = 7$ ns (FWHM), $E_{IN} = 0.417$ μJ, $T_L = 47.5\%$, $L = 50$ μm]. A sample filled with nigrosine dissolved in water is placed at the position corresponding to the minimum of the closed-aperture Z-scan curve.

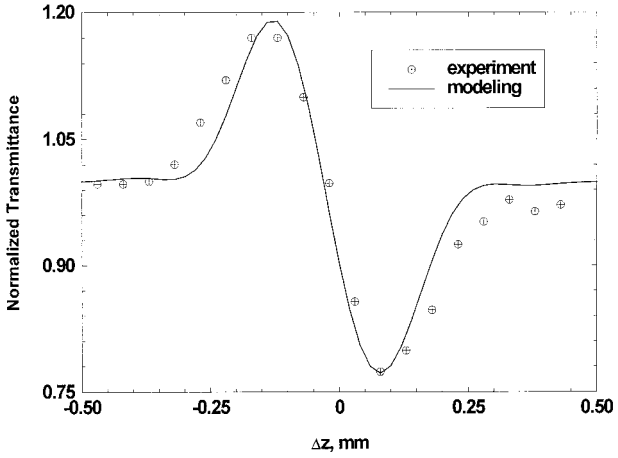

Fig. 13. Closed-aperture Z-scan of nigrosine in water. Flat-top input beam geometry was used. Parameters of the system are the same as for Fig. 12.

these by expanding an initially Gaussian beam and sending it through a finite aperture that clips the beam to approximate a cylindrically symmetric flat-top beam. Figure 12 shows a comparison of the calculated radial fluence distribution with the experimental distribution for a flat-top beam focused into a solution of nigrosine dye dissolved in water. The detector in this experiment is located at the plane where the size of the beam is equal to the size of a clipping aperture (note that an extra lens is placed after the sample; see the output lens in Fig. 1). The sample is placed at the position corresponding to the minimum of the closed-aperture Z-scan curve (Fig. 13). For low values of input energy the beam shape on the detector is just a replica of the input top-hat profile (with minor diffraction ripples). However, by increasing the input energy of the laser beam we introduce a certain amount of nonlinear phase shift. For a defocusing nonlinearity this results in distortion of the beam profile on the detector making it ringlike. In this case most of the energy is concentrated in the wings. Therefore it is possible to eliminate a large portion of the output energy by placing a suitable aperture in the beam. In this way the nonlinear thermal effect in liquid solvents could be used to enhance the performance of the optical limiter, i.e., block energy at high inputs. However, ideally, the aperture should have no effect on the low-energy input beam, and thus such an approach has a significant drawback. For a self-focusing nonlinearity the profile becomes more sharply peaked with the sample placed after the focus; however, with the sample placed prior to focus it also has a ring shape.

6. Conclusions

We have developed computationally efficient computer codes for modeling the propagation of high-irradiance laser pulses through thick (many diffraction lengths) nonlinear optical materials including several nonlinear mechanisms relevant to optical limiting. In addition to the inclusion of both ultrafast nonlinear absorption and refraction, we have included the effects of excited states on both the absorption and the refraction. These nonlinearities accumulate with time within a laser pulse. Computationally this requires the code to remember the effects induced by previous parts of the laser pulse. We have also included the effects of thermal lensing with the added complication of the acoustic waves generated by linear and nonlinear absorption. This requires simultaneous solutions to two wave equations and is computationally intensive; however, this is still within the range of modern PC's. To produce a more time-efficient code we have studied the region of validity of an approximate solution to the acoustic-wave equation. We model the limiting performance of a SiNc–toluene limiter for nanosecond input pulses including transient thermal effects and show how one can suppress thermal defocusing by placing the limiter in front of the focal plane. The attractive features of this beam propagation code is its speed, accessibility (runs on PC's), and exact modeling of time-dependent nonlinear self-action phenomena (e.g., excited-state nonlinearities and transient thermal effects). Comparisons between the output of our program with experiments are given for the most computationally challenging geometries (thick samples, top-hat beams) and NLO responses (coupled RSA and thermal refraction).

Appendix A

When a liquid or gas medium absorbs energy from a laser beam, the result is changes of density, temperature, pressure, and fluid velocity. The system of equations describing such changes can be derived from the three fundamental laws of hydrodynamics[48]:

$$\frac{\partial \rho}{\partial t} + \nabla(\rho u) = 0, \tag{A1}$$

the continuity or conservation of mass equation,

$$\rho\left[\frac{\partial u}{\partial t} + (u\nabla)u\right] + \nabla p + \eta\nabla^2 u + \left(\zeta + \frac{\eta}{3}\right)\nabla(\nabla u) = \nabla F, \tag{A2}$$

the Navier–Stokes or conservation of momentum equation, and

$$\rho T\left(\frac{\partial s}{\partial t} + u\nabla s\right) = \nabla(\kappa\nabla T) + \sigma_{ik}{}'\frac{\partial u_i}{\partial x_k} + Q, \tag{A3}$$

the heat balance or conservation of energy equation. Here ρ is the density, p is the pressure, T is the temperature, s is the entropy, u is the fluid velocity of the media, κ is the thermal conductivity, and η, ζ are the effective viscosities. The pressure induced by the electrostrictive effect is given by[29]

$$F(r, t) = \rho\left(\frac{\partial n}{\partial \rho}\right)_T \frac{I(r, t)}{c}. \tag{A4}$$

$$Q(r, t) = \alpha_L I(r, t) \tag{A5}$$

is the heat generated by absorption of the laser pulse with irradiance $I(r, t)$. c is the velocity of light in vacuum, n is the index of refraction, and α_L is the linear absorption coefficient of the medium (the formalism can clearly be extended for the case of nonlinear absorption in which case the expression for Q will include, e.g., $\beta_2 I^2$ for 2PA). Combining the continuity of Eq. (A1) with the Navier–Stokes equation in Eq. (A2) and expressing all the quantities in terms of the local density ρ' and temperature change T' (where ρ' and T' are assumed to be small quantities compared with equilibrium values ρ and T), we obtain

$$\left(-\frac{\partial^2}{\partial t^2} + \frac{C_S{}^2}{\gamma}\nabla^2 + \frac{\eta}{\rho}\frac{\partial}{\partial t}\nabla^2\right)\rho' + \frac{C_S{}^2\beta\rho}{\gamma}\nabla^2 T' = \frac{\gamma^e}{2nc}\nabla^2 I, \tag{A6}$$

where $C_S = [(\partial p/\partial\rho)_S]^{1/2}$ is the adiabatic velocity of sound, $\gamma = c_p/c_V$ is the ratio between constant pressure and constant volume heat capacities, $\beta = -(1/V)(\partial V/\partial T)_p$ is the coefficient of thermal expansion, and $\gamma^e = \rho(\partial n^2/\partial\rho)_T$ is the electrostrictive coupling constant, which can be estimated by use of Lorentz–Lorenz law as $(n^2 - 1)(n^2 + 2)/3$. Combining the heat transfer equation in Eq. (A3) with the continuity equation in Eq. (A1) and eliminating all the variables except density and temperature variations, we obtain

$$\left(\rho c_V\frac{\partial}{\partial t} - \kappa\nabla^2\right)T' - \frac{c_p - c_V}{\beta}\frac{\partial\rho'}{\partial t} = \alpha_L I. \tag{A7}$$

The resultant Eqs. (A6) and (A7) are usually used for analysis of the hydrodynamics of a liquid media while interacting with a laser beam.[35–37]

If the time scale of the laser pulse is of the order of a few nanoseconds, the diffusion term in Eq. (A7) can be ignored, as the characteristic time of thermal diffusion is usually a few orders of magnitude longer than a pulse width.[30] If we take the derivative with time of Eq. (A6) and the Laplacian of Eq. (A7), the two equations can be combined into one:

$$\frac{\partial}{\partial t}\left(\frac{\partial^2\rho'}{\partial t^2} - C_S{}^2\nabla^2\rho'\right) = \frac{C_S{}^2\beta\alpha_L}{c_p}\nabla^2 I - \frac{\gamma^e}{2nc}\frac{\partial}{\partial t}\nabla^2 I, \tag{A8}$$

which is the wave equation for the density perturbation that is due to the two effects (two source terms on the right side)—absorption of the light energy and the electrostrictive effect.

In absorptive liquid solutions, electrostriction is usually the smaller effect, and thus we ignore the second source term in Eq. (A8). Here we also assume that the light energy absorbed is converted into kinetic energy of the molecules on a time scale shorter than the pulse itself. This is usually true for relaxation of vibration transitions of molecules in liquids.[35,36]

The refractive index is related to the density and temperature changes as

$$\Delta n = \left(\frac{\partial n}{\partial\rho}\right)_T\rho' + \left(\frac{\partial n}{\partial T}\right)_\rho T' = \frac{\gamma^e}{2n\rho}\rho' + \left(\frac{\partial n}{\partial T}\right)_\rho T'. \tag{A9}$$

For most liquids the refractive index is generally more sensitive to density variations than to temperature variations, and therefore the last term in Eq. (A9) can be neglected.

Thus the wave equation for the index change that is due to the photoacoustic effect can be written as

$$\frac{\partial^2(\Delta n)}{\partial t^2} - C_S{}^2\nabla^2(\Delta n) = \frac{\gamma^e}{2n\rho}\frac{\beta C_S{}^2}{c_p}\int_{-\infty}\nabla^2[\alpha_L I(r, t')]\mathrm{d}t'. \tag{A10}$$

The source factor in Eq. (A10) can be expressed in terms of the temperature change. The simplified heat balance equation in Eq. (A3) for a static liquid for the case when the heat flow is mainly due to thermal conduction is

$$\rho c_p\frac{\partial T}{\partial t} - \kappa\nabla^2 T = \alpha_L I \tag{A11}$$

and can be integrated for nanosecond time scales (ignoring temperature diffusion) to yield

$$T'(r, t) = \frac{1}{\rho c_p}\int_{-\infty}\alpha_L I(r, t')\mathrm{d}t'. \tag{A12}$$

Combining Eqs. (A10) and (A12) we obtain the final form of the acoustic-wave equation for refractive-index changes:

$$\frac{\partial^2(\Delta n)}{\partial t^2} - C_S{}^2\nabla^2(\Delta n) = C_S{}^2\frac{\gamma^e\beta}{2n}\nabla^2 T'(r, t). \tag{A13}$$

The refractive-index change in the paraxial approximation (close to the laser beam axis) for times longer

than the acoustic transit time ($\tau_p > \tau_{ac} = w/C_S$) can be reduced to[29]

$$\Delta n = \left(\frac{dn}{dT}\right) T', \tag{A14}$$

where $(dn/dT) = \gamma^e \beta / 2n$ [if only the absorptive source term in Eq. (A8) is taken into account] and the temperature change is given by Eq. (A12). The expression in Eq. (A14) is a commonly used approximation called the thermal lensing effect, which is usually applied for much longer time scales $C_S t/w > 1$ (microseconds up to cw) when the index change is controlled by thermal diffusion. This coefficient in Eq. (A14) (dn/dT) is called the thermo-optic coefficient, and it has been measured for many organic solvents. The actual thermal lens induced by the density perturbation in the material is an aberrated replica of the one in Eq. (A14) because this approximation can only be made for near-axis index changes. Nevertheless, it was shown[41] that Eq. (A14) can be used to describe the dynamics of the refractive-index change in the transient regime if the characteristic length of the acoustic wave generated by the laser beam ($C_S \tau_p$) is larger than the beam size (the acoustic wave has enough time to travel across the beam during the pulse).

This research was performed with support from the Office of Naval Research, grant N00014-97-1-0936, and the Naval Air Warfare Center Joint Service Agile Program, contract N00421-98-C-1327.

References

1. H.-P. Nolting and R. Marz, "Results of benchmark tests for different numerical BPM algorithms," IEEE J. Lightware Technol. **13,** 216–224 (1995) and references therein.
2. G. P. Agrawal, *Nonlinear Fiber Optics* (Academic, New York, 1989).
3. M. D. Feit and J. A. Fleck, Jr., "Simple method for solving propagation problems in cylindrical geometry with fast Fourier transforms," Opt. Lett. **14,** 662–664 (1989).
4. J. A. Fleck, Jr., J. R. Morris, and M. D. Feit, "Time-dependent propagation of high energy laser beams through the atmosphere," Appl. Phys. **10,** 130–160 (1976).
5. S. Hughes, J. M. Burzer, G. Spruce, and B. S. Wherrett, "Fast Fourier transform techniques for efficient simulation of Z-scan measurements," J. Opt. Soc. Am. B **12,** 1888–1893 (1995).
6. E. A. Sziklas and E. Siegman, "Mode calculations in unstable resonators with flowing saturable gain. 2: Fast Fourier transform method," Appl. Opt. **14,** 1874–1889 (1975).
7. D. J. Hagan, T. Xia, A. A. Said, T. H. Wei, and E. W. Van Stryland, "High dynamic range passive optical limiters," Int. J. Nonlinear Opt. Phys. **2,** 483–501 (1993); L. W. Tutt and T. F. Boggess, "A review of optical limiting mechanisms and devices using organics, fullerenes, semiconductors and other materials," Prog. Quantum Electron. **17,** 299–338 (1993).
8. D. Kovsh, S. Yang, D. J. Hagan, and E. W. Van Stryland, "Software for computer modeling of laser pulse propagation through the optical system with nonlinear optical elements," in *Nonlinear Optical Liquids for Power Limiting and Imaging*, C. M. Lawson, ed., Proc. SPIE **3472,** 163–177 (1998).
9. C. T. Law and G. A. Swartzlander, Jr., "Implementation of a package for optical limiter modeling," in *Nonlinear Optical Liquids and Power Limiters*, C. M. Lawson, ed., Proc. SPIE **3146,** 95–106 (1997).
10. M. Sheik-bahae, A. A. Said, and E. W. Van Stryland, "High-sensitivity, single-beam n_2 measurements," Opt. Lett. **14,** 955–957 (1989).
11. R. W. Boyd, *Nonlinear Optics* (Academic, New York, 1992).
12. G. R. Hadley, "Wide-angle beam propagation using Padé approximant operators," Opt. Lett. **17,** 1426–1428 (1992).
13. W. H. Southwell, "Validity of the Fresnel approximation in the near field," J. Opt. Soc. Am. **71,** 7–14 (1981).
14. W. H. Press, B. P. Flannery, S. A. Teukolsky, and W. T. Vetterling, *Numerical Recipes. The Art of Scientific Computing* (Cambridge U. Press, Cambridge, UK, 1986).
15. S. T. Hendow and S. A. Shakir, "Recursive numerical solution for nonlinear wave propagation in fibers and cylindrically symmetric systems," Appl. Opt. **25,** 1759–1764 (1986).
16. T. Xia, "Modeling and experimental studies of nonlinear optical self-action," Ph.D. dissertation (University of Central Florida, Orlando, Fla., 1994).
17. T. H. Wei, D. J. Hagan, M. J. Sence, E. W. Van Stryland, J. W. Perry, and D. R. Coulter, "Direct measurements of nonlinear absorption and refraction in solutions of phthalocyanines," Appl. Phys. B **54,** 46–51 (1992).
18. P. Miles, "Bottleneck optical limiters: the optimal use of excited-state absorbers," Appl. Opt. **33,** 6965–6979 (1994).
19. H. S. Nalwa and S. Miyata, eds., *Nonlinear Optics of Organic Molecules and Polymers* (CRC Press, Boca Raton, Fla., 1997); J. W. Perry, "Organic and metal-containing reverse saturable absorbers for optical limiters," Chap. 13, pp. 813–840.
20. T. Xia, D. J. Hagan, A. Dogariu, A. A. Said, and E. W. Van Stryland, "Optimization of optical limiting devices based on excited-state absorption," Appl. Opt. **36,** 4110–4122 (1997).
21. O. V. Przhonska, J. H. Lim, D. J. Hagan, E. W. Van Stryland, M. V. Bondar, and Y. L. Slominsky, "Nonlinear light absorption of polymethine dyes in liquid and solid media," J. Opt. Soc. Am. B **15,** 802–809 (1998).
22. D. C. Hutchings, M. Sheik-Bahae, D. J. Hagan, and E. W. Van Stryland, "Kramers-Kronig relations in nonlinear optics," Opt. Quantum Electron. **24,** 1–30 (1992).
23. J. P. Gordon, R. C. C. Leite, R. S. Moore, S. P. S. Porto, and J. R. Whinnery, "Long-transient effects in lasers with inserted liquid samples," J. Appl. Phys. **36,** 3–8 (1965).
24. S. A. Akhmanov, D. P. Krindach, A. V. Migulin, A. P. Sukhorukov, and R. V. Khokhlov, "Thermal self-action of laser beams," IEEE J. Quantum Electron. **QE-4,** 568–575 (1968).
25. C. K. N. Patel and A. C. Tam, "Pulsed optoacoustic spectroscopy of condensed matter," Rev. Mod. Phys. **53,** 517–550 (1981).
26. J. N. Hayes, "Thermal blooming of laser beams in fluids," Appl. Opt. **11,** 455–461 (1972).
27. A. J. Twarowski and D. S. Kliger, "Multiphoton absorption spectra using thermal blooming. I. Theory," Chem. Phys. **20,** 253–258 (1977).
28. S. J. Sheldon, L. V. Knight, and J. M. Thorne, "Laser-induced thermal lens effect: a new theoretical model," Appl. Opt. **21,** 1663–1669 (1982).
29. P. R. Longaker and M. M. Litvak, "Perturbation of the refractive index of absorbing media by a pulsed laser beam," J. Appl. Phys. **40,** 4033–4041 (1969).
30. G. Liu, "Theory of the photoacoustic effect in condensed matter," Appl. Opt. **21,** 955–960 (1982).
31. C. A. Carter and J. M. Harris, "Comparison of model describing the thermal lens effect," Appl. Opt. **23,** 476–481 (1984).
32. A. M. Olaizola, G. Da Costa, and J. A. Castillo, "Geometrical interpretation of a laser-induced thermal lens," Opt. Eng. **32,** 1125–1130 (1993).
33. F. Jurgensen and W. Schroer, "Studies on the diffraction image of a thermal lens," Appl. Opt. **34,** 41–50 (1995).
34. S. Wu and N. J. Dovichi, "Fresnel diffraction theory for steady-

state thermal lens measurements in thin films," J. Appl. Phys. **67,** 1170–1182 (1990).
35. S. R. J. Brueck, H. Kildal, and L. J. Belanger, "Photo-acoustic and photo-refractive detection of small absorptions in liquids," Opt. Commun. **34,** 199–204 (1980).
36. J.-M. Heritier, "Electrostrictive limit and focusing effects in pulsed photoacoustic detection," Opt. Commun. **44,** 267–272 (1983).
37. P. Brochard, V. Grolier-Mazza, and R. Cabanel, "Thermal nonlinear refraction in dye solutions: a study of the transient regime," J. Opt. Soc. Am. B **14,** 405–414 (1997).
38. J.-G. Tian, C. Zhang, G. Zhang, and J. Li, "Position dispersion and optical limiting resulting from thermally induced nonlinearities in Chinese tea," Appl. Opt. **32,** 6628–6632 (1993).
39. Y. M. Cheung and S. K. Gayen, "Optical nonlinearities of tea studied by Z-scan and four-wave mixing techniques," J. Opt. Soc. Am. B **11,** 636–643 (1994).
40. J. Castillo, V. P. Kozich, and A. Marcano O., "Thermal lensing resulting from one- and two-photon absorption studied with a two-color time-resolved Z scan," Opt. Lett. **19,** 171–173 (1994).
41. D. I. Kovsh, D. J. Hagan, and E. W. Van Stryland, "Numerical modeling of thermal refraction in liquids in the transient regime," Opt. Exp. **4,** 315–327 (1999).
42. M. Sheik-Bahae, A. A. Said, T. Wei, D. J. Hagan, and E. W. Van Stryland, "Sensitive measurements of optical nonlinearities using a single beam," IEEE J. Quantum Electron. **26,** 760–769 (1990).
43. A. A. Said, T. Xia, D. J. Hagan, A. Wajsgrus, S. Yang, D. Kovsh, M. A. Decker, S. Khodja, and E. W. Van Stryland, "Liquid-based multicell optical limiter," in *Nonlinear Optical Liquids*, C. M. Lawson, ed., Proc. SPIE **2853,** 158–169 (1996).
44. B. L. Justus, Z. H. Kafafi, and A. L. Huston, "Excited-state absorption-enhanced thermal optical limiting in C_{60}," Opt. Lett. **18,** 1603–1605 (1993).
45. B. L. Justus, A. J. Campillo, and A. L. Huston, "Thermal-defocusing/scattering optical limiter," Opt. Lett. **19,** 673–675 (1994).
46. K. Mansour, E. W. Van Stryland, and M. J. Soileau, "Nonlinear properties of carbon-black suspensions (ink)," J. Opt. Soc. Am. B **9,** 1100–1109 (1992).
47. R. R. Michael and C. M. Lawson, "Nonlinear transmission and reflection at a dielectric-carbon microparticle suspension interface," Opt. Lett. **17,** 1055–1057 (1992).
48. D. Landau and E. M. Lifshitz, *Course of Theoretical Physics: Fluid Mechanics* (Pergamon, New York, 1996), Vol. 6.